Recurrent marine anoxia in the Paleo-Tethys linked to constriction of seaways during the Early Triassic

Yuyang Wu, Alexandre Pohl, Li Tian, Jacopo Dal Corso, Ying Cui, Daoliang Chu, Jinnan Tong, Huyue Song, Hanchen Song, Haijun Song

Recurrent marine anoxia in the Paleo-Tethys linked to constriction of seaways during the Early Triassic

Yuyang Wu [a], Alexandre Pohl [b], Li Tian [a], Jacopo Dal Corso [a], Ying Cui [c], Daoliang Chu [a], Jinnan Tong [a], Huyue Song [a], Hanchen Song [a], Haijun Song [a,*]

[a] State Key Laboratory of Biogeology and Environmental Geology, School of Earth Sciences, China University of Geosciences, Wuhan 430074, China
[b] Biogéosciences, UMR 6282 CNRS, Université de Bourgogne, 6 Boulevard Gabriel, Dijon 21000, France
[c] Department of Earth and Environmental Studies, Montclair State University, Montclair, NJ 07043, USA

ARTICLEINFO

Editor: Dr H Bao

Keywords:
Ocean deoxygenation Hypoxia
Permian-Triassic Paleogeography
Earth system modeling

ABSTRACT

Recurrent global marine anoxia marked the Early Triassic in the aftermath of the Permian-Triassic mass extinction. Growing evidence suggests contrasting redox histories across regions, with differing durations and intensities of anoxic conditions, but proposed climate-induced mechanisms for marine anoxia cannot fully explain these contrasting redox histories. Here, we test the impacts of changes in continental configuration on the redox conditions during the Early Triassic. We combine redox proxy data and Earth system model simulations, together with geological evidence for continental configuration in the Paleo-Tethys, showing that regional dif- ferences in redox conditions developed in the Early Triassic, primarily as a consequence of restricted seaways. In the model, a reduction in the depth of the seaways connecting the Paleo-Tethys and Panthalassa oceans leads to deoxygenation of the seafloor in the restricted Paleo-Tethys, aligning with redox proxy data. Ocean deoxygen- ation in the Paleo-Tethys primarily arises from the weakening of regional ocean ventilation due to the disruption of deep-water flow across the seaways. In contrast, simulations show that changes in continental configuration prompted ocean ventilation and oxygenation in some regions of the Panthalassa and Neo-Tethys, which explains the earlier reoxygenation of these basins before the late Early Triassic, as indicated by redox proxies. These varying spatial patterns of the redox landscape throughout the Early to Middle Triassic may help account for the delayed recovery of marine taxonomic diversity until the Middle Triassic in the Paleo-Tethys, contrastingwith the quicker recovery observed in other regions before the Middle Triassic.

Introduction

The delayed recovery of marine biodiversity after the Permian- Triassic mass extinction (PTME) is thought to have been driven by recurrent marine anoxia related to long-lasting global warming in the Early Triassic (Payne et al., 2004; Wignall et al., 2010; Sun et al., 2012; Song et al., 2012; Grasby et al. 2013). Uranium isotopes, a proxy for the global extent of seafloor anoxia, show multiple negative shifts throughout the Early Triassic that indicate recurrent expansions of anoxic seafloor areas persisting until the Early-Middle Triassic transition (Lau et al., 2016; Zhang et al., 2018a). However, increasing evidence from local redox proxies highlights substantial variations in the duration and intensity of anoxic conditions across regions. For example, recurrent marine anoxia extended until the Early-Middle Triassic transition in the eastern Paleo-Tethys and central Panthalassa (Isozaki, 1997; Wignall et al., 2010; Tian et al., 2014), and the marine anoxia in the northern Panthalassa was maintained until the middle Spathian (Grasby et al., 2013). In contrast, the southern Panthalassa and Neo-Tethys became oxic before the late Early Triassic (Spathian) (Clarkson et al., 2016; Grasby et al., 2021; Sun et al., 2021).

The results from Earth system modeling provide various explana- tions for marine anoxia during the PTME. Some models suggest a stratified ocean with weakened vertical mixing due to global warming (Kiehl and Shields, 2005; Penn et al., 2018), whereas others propose enhanced export productivity, caused by increased nutrient inputs (Meyer et al., 2008; Winguth and Winguth, 2012) or warming-induced increase in microbial metabolism leading to the expansion of euxinic waters onto continental shelves (Hülse et al., 2021). These explanations, though differing in their underlying causes, all relate to global warming triggered by massive carbon emissions (e.g., Burgess et al. 2017, Wu et al. 2023). These warming-induced mechanisms are also important triggers for anoxic conditions in the post-PTME, due to persistent warming during the Early Triassic (Sun et al., 2012). However, they cannot fully explain the spatial variations in post-PTME anoxic condi- tions. The fundamental mechanisms behind the spatial variations in post-PTME anoxic conditions during the Early Triassic remain poorly understood.

To fill this gap, we first compile redox proxy data to show the spatial differences in redox conditions that developed during the Early Triassic. Meanwhile, we assemble sedimentological, paleomagnetic and magmatic information have been assembled to map out a constriction of the seaways between the Paleo-Tethys and Panthalassa oceans. We then quantify the impact of seaway changes on ocean redox conditions using Earth system model simulations to reveal the fundamental mechanisms behind the spatial variations in anoxic conditions during the Early Triassic. Consistent with compiled redox proxy dataset, the modeling shows that constriction of the seaways led to contrasting responses of ocean oxygenation in the Early Triassic, with dissolved oxygen con- centrations increasing everywhere except in the Paleo-Tethys where severe deoxygenation was maintained.

Methods

Proxy data compilation

Published carbonate uranium isotopes ($\delta^{238}U_{carb}$) and carbon iso- topes ($\delta^{13}C_{carb}$) from 11 sections were compiled: Guandao (Payne et al.,

* Corresponding author.
E-mail address: haijunsong@cug.edu.cn (H. Song).

https://doi.org/10.1016/j.epsl.2024.118882
Received 1 April 2024; Received in revised form 30 June 2024; Accepted 4 July 2024

2004; Lau et al., 2016), Dajiang (Payne et al., 2004; Lau et al., 2016), Dawen (Payne et al., 2004; Brennecka et al., 2011), Zuodeng (Zhang et al., 2019), Jiarong (Zhao et al., 2020), Zal (Zhang et al., 2018a), Daxiakou (Elrick et al., 2017), Jesmond (Zhang et al., 2019), Kamura (Zhang et al., 2018b), Taskent (Lau et al., 2016) and Gartnerkofel 1 (Zhang et al., 2020). The age models for each profile were calculated by

negative carbon isotope excursions (N1 to N4), positive carbon isotope excursions (P1 to P4) from Song et al. (2013) and the Triassic timescale (Tong et al., 2019) that is based on a combination of zircon U-Pb dating studies (Supplementary Material). Pyrite framboid, redox-sensitive trace elements (e.g., Mo, U) and Fe speciation data were collected to recon- struct the local redox changes. A total of 42 local redox profiles were collected from various oceanic regions (Supplemental Data S1). Seven relatively continuous profiles from different oceanic regions were cho- sen to exhibit spatial variances in the durations and intensities of anoxic conditions during the Early-Middle Triassic (Figs. 1B, S1).

Earth system modeling

To quantify the impact of seaway configuration on ocean oxygena- tion in the Paleo-Tethys during the Triassic, we use 'cGENIE' in this study, an Earth system model of intermediate complexity. It is composed of a 3-D dynamic ocean circulation model with a 2-D energy and moisture balance model of the atmosphere, a dynamic thermodynamic sea-ice model (Edwards and Marsh, 2005), and a representation of the biogeochemical cycling of elements and isotopes in the ocean (Ridgwell et al., 2007). The model incorporates Arrhenius-type temper- ature-dependent scheme for the remineralization of organic matter (Crichton et al., 2021). Nutrient inventories, which are crucial for con- trolling the biological pump, have been simplified in our simulations by including only phosphate (Meyer et al., 2016).

In the absence of accurate constraints on the geometry and depth of the seaways in study region, we designed three idealized scenarios (Fig. 2D): scenario 1 with very deep seaways (water depth ~4000 m) between the Paleo-Tethys and the Panthalassa; scenario 2 with shallow seaways (water depth set as ~500 m) and scenario 3 with closed sea- ways between the Paleo-Tethys and the Panthalassa (seaways between the Neo-Tethys and the Panthalassa are kept open in all scenarios). We implemented our three scenarios of continental configuration

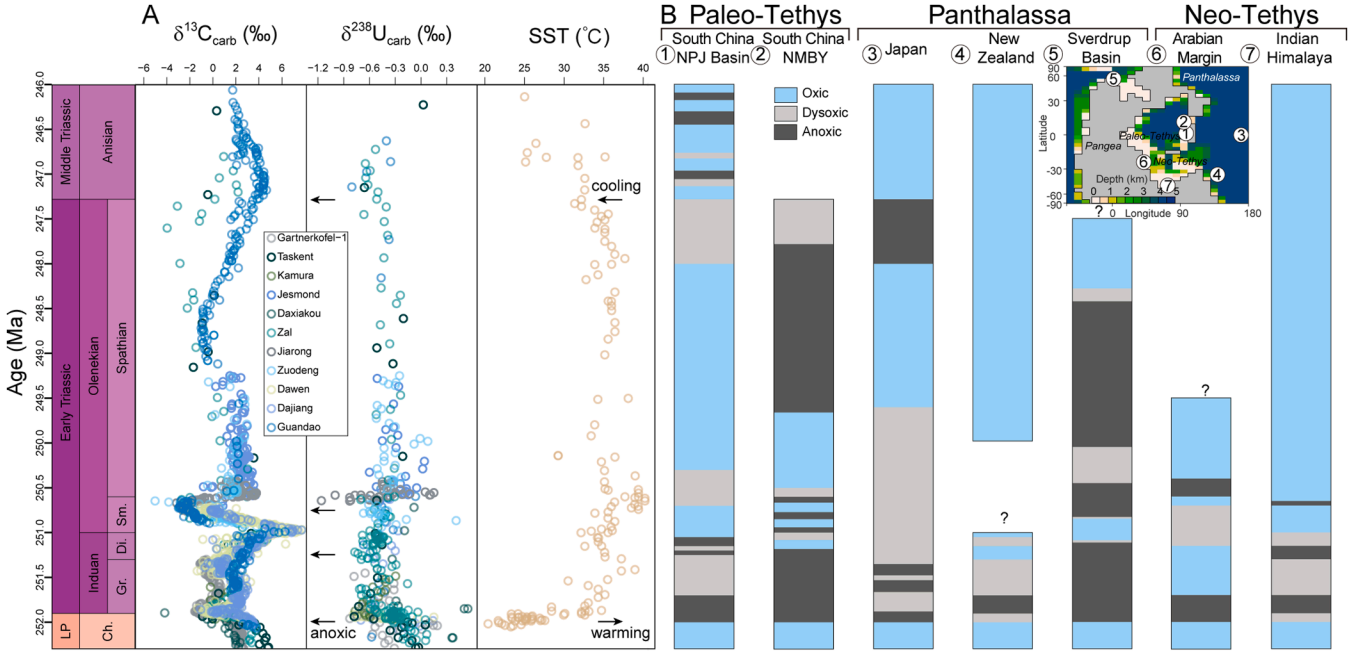

Fig. 1. Summary of latest Permian to early Middle Triassic proxy data. (A) Compiled marine carbonate carbon isotopes and uranium isotopes (Supplemental Data S1) and sea surface temperature (SST) based on conodont oxygen isotopes (Sun et al., 2012; Trotter et al., 2015). (B) Local redox history from seven regions (42 records summarized in the Supplemental Data S1): the Nanpanjiang (NPJ) Basin and northern marginal basin of the Yangtze Platform (NMBY) from South China (Tian et al., 2014; Saito et al., 2014; Huang et al., 2017), Japan (Wignall et al., 2010), Sverdrup basin (Grasby et al., 2013), Arabian Margin (Clarkson et al., 2016), Indian Himalaya (Sun et al., 2021), and New Zealand (Grasby et al., 2021). Location of seven regions shown on top of paleobathymetry represented at the model resolution. Oxic, dysoxic and anoxic (containing ferruginous and euxinic) conditions are distinguished. The age and stratigraphic correlation are based on the Triassic timescale (Tong et al., 2019), conodont zones and carbon isotope profiles (Supplemental Material). LP–late Permian; Ch–Changhsingian, Gr–Griesbachian, Di–Dienerian, Sm–Smithian.

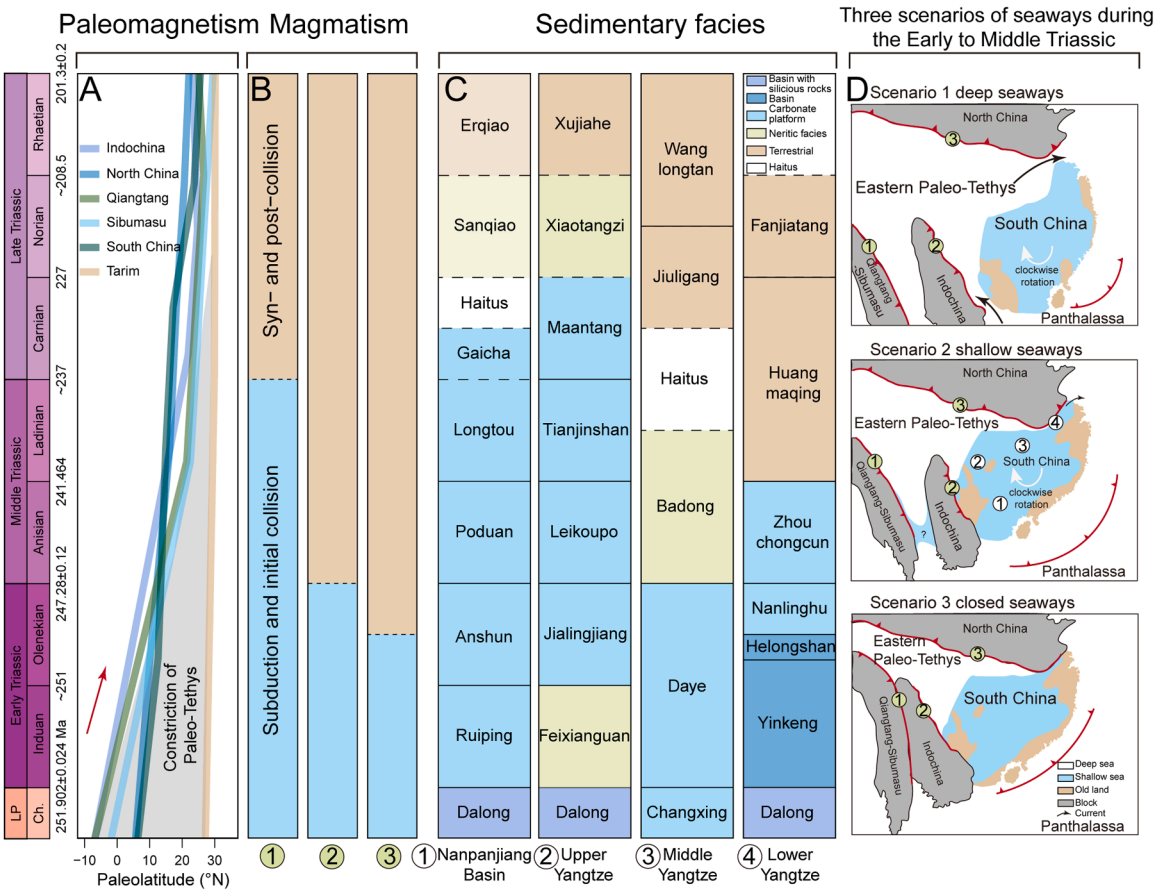

Fig. 2. The Triassic constriction of seaways in the eastern Paleo-Tethys. (A) Paleolatitude of seven blocks obtained by paleomagnetism showing gradual constriction of the Paleo-Tethys (Huang et al., 2018; Zhu et al., 2022). (B) Magmatism of sutures showing different stages of continental collision (Wang et al., 2018; Hu et al., 2020). 1. Changning-Menglian suture; 2. Ailaoshan-Song Ma suture; 3. Qinglin-Dabie suture. (C) Triassic sedimentary facies change from marine to terrestrial facies in South China (Tong et al., 2021). (D) Assumed three scenarios of seaways in the eastern Paleo-Tethys. The paleogeography is modified from Feng et al. (1997) and Duan et al. (2020).

(Fig. 3A–C) on the model 36 36 equal-area horizontal grid with 16 depth levels in the ocean. These scenarios involved slight adjustments to the end-Permian continental configuration and bathymetry used in previous studies (e.g., Meyer et al. 2008, Hülse et al. 2021) while keeping planetary albedo, wind stress, and velocity unchanged, using the 'muffingen' open-source software. The three main experiments were run using an atmospheric oxygen concentration set to modern (20.95%), 10 × preindustrial atmospheric CO_2 levels representing the warm con- ditions roughly similar to the Early Triassic maximum CO_2 levels (Joachimski et al., 2022) and a mean ocean phosphate concentration ($[PO_4]$) set to 1.5 × modern levels.

We conducted sensitivity tests on seaway depth, atmospheric CO_2 levels and oceanic $[PO_4]$, through an ensemble of 26 different sensitivity experiments, because of dynamic atmospheric CO_2 levels, oceanic redox conditions and seaway depth during the Early Triassic (Fig. 1), such as a drop of CO_2 levels during the late Early Triassic (Joachimski et al., 2022). An ensemble of 12 sensitivity simulations was run using scenario 2 for various values of atmospheric pCO_2 (2 ×, 5 ×, 10 ×, 20 × the preindustrial atmospheric concentration of 280 ppm) and oceanic $[PO_4]$ (1.0 , 1.5 , 2.0 modern levels). We further conducted an ensemble of 14 additional experiments to explore the sensitivity of our results to the depth of the seaways (from 0 to 4000 m) that connect the Paleo-Tethys and Panthalassa oceans in scenario 2. All experiments were run for 10 kyr in a closed system to ensure equilibrium.

Results and discussion

Global and local ocean redox changes

Compiled $\delta^{238}U_{carb}$ data show pronounced negative shifts, featuring four negative peaks from the Early Triassic to early Middle Triassic (Fig. 1A; Lau et al., 2016; Zhang et al., 2018a), suggesting that wide- spread seafloor anoxia persisted until the Anisian. However, local redox proxy data (pyrite framboid, redox-sensitive trace element and Fe speciation) from seven regions reveal significant temporal variations in the local demise of anoxic marine conditions spanning over 4 Myr, from the early Spathian to the Anisian (Fig. 1B). Marine anoxia across the Smithian-Spathian boundary is widely recorded but interrupted by a phase of global oxygenation during the early-middle Spathian, as evi- denced by the development of marine red beds (e.g., Li et al. 2023). Recurrent marine anoxia continued until the Early-Middle Triassic transition exclusively in the eastern Paleo-Tethys (Tian et al., 2014; Huang et al., 2017) and central Panthalassa (Takahashi et al., 2009, 2015; Wignall et al., 2010). Notably, the succession of South China re- cords recurrent anoxia persisting until the Anisian in the Nanpanjiang Basin, evidenced by the occurrence of pyrite framboids (e.g., Huang et al. 2017), Ce anomalies in conodonts (Song et al., 2012) and enrichment of redox-sensitive trace elements such as Mo, U, and V (e.g., Saito et al. 2014). In contrast, redox-sensitive trace metals, pyrite framboid, Fe speciation data from New Zealand in Southern Panthalassa and Neo-Tethys indicate that benthic waters recovered more quickly before the late Early Triassic (Spathian) (Clarkson et al., 2016; Grasby

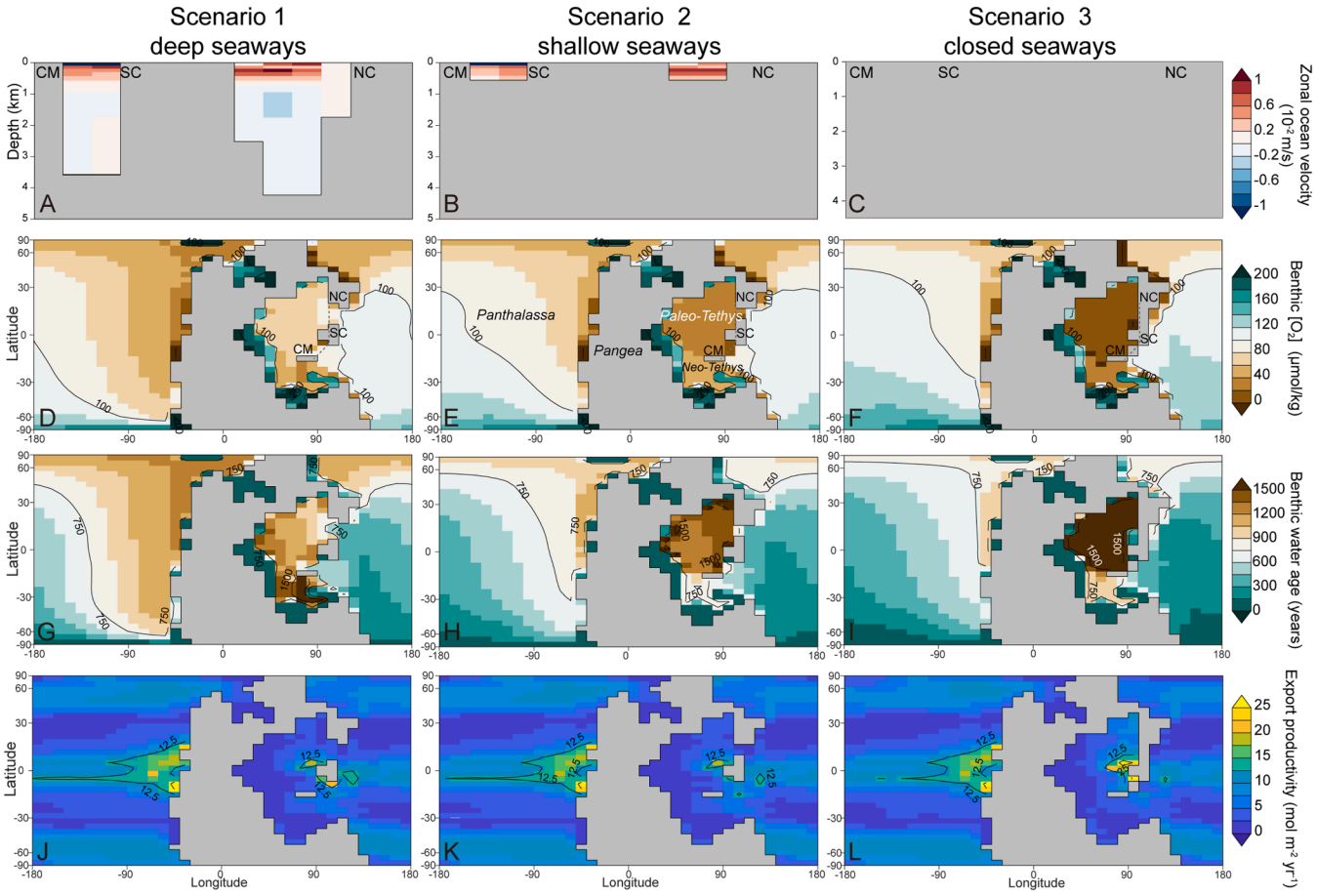

Fig. 3. Sensitivity of ocean circulation and ocean [O_2] to the depth of seaways in an Earth system model. (A–C) Zonally-averaged ocean velocity across transects of seaways in the eastern Paleo-Tethys. Positive values indicate eastward transport from the Paleo-Tethys to the Panthalassa. Negative values indicate westward transport from the Panthalassa to the Paleo-Tethys. (D–F) Simulated benthic [O_2]. (G–I) Simulated benthic water age (defined as the time since a parcel of water last reached the ocean surface), used here to illustrate ocean ventilation. (J–L) Simulated surface export production. SC—South China, NC—North China, CM—Cimmerian.

et al., 2021; Sun et al., 2021). Despite the occasional discontinuity in some redox records, a total of 42 redox records further delineates the varying spatial patterns of the redox landscape during the Early Triassic (Supplementary Data S1).

Constriction of seaways in the eastern Paleo-Tethys

Constriction of the eastern Paleo-Tethys seaways mainly occurred from the Early to Middle Triassic (Fig. 2). During the Early Triassic, the Paleo-Tethys was a restricted ocean surrounded by landmasses on all sides except to the east, where it interconnected with the Panthalassa through a series of seaways situated between several continental blocks, namely South China, North China, Indochina and Cimmerian blocks (Şengör and Atayman, 2009; Metcalfe, 2021; Scotese, 2021). Paleo- magnetic evidence from these blocks (Huang et al., 2018; Zhu et al., 2022) and magmatic activity along sutures (Wang et al., 2018; Hu et al., 2020) indicate a northward drift of these blocks. This movement caused subduction and initial collisions among South China, North China, Indochina, and Cimmerian blocks from the late Permian to the Middle Triassic, leading to an increasingly restricted Paleo-Tethys. Intensified dolomitization during the PTME in the Paleo-Tethys, indicated by rapid changes in seawater magnesium isotopes (Hu et al., 2021), further supports these increasingly restricted conditions. Sedimentary facies records in South China reveal a transition from deep-water to shallow-water sediments beginning in the late Early Triassic, indicative of an initial collision between South China and North China (Tong et al.,

2021). This collision, occurring earlier in the eastern part, generated terrestrial sediments in the Lower Yangtze region by the late Middle Triassic (Fig. 2). In the absence of accurate constraints on the geometry and depth of the seaways in study region, we consider and test hereafter three scenarios capturing the range of possible seaway states during the Early to Middle Triassic (Fig. 2D): scenario 1 with very deep seaways (deep ocean) between the Paleo-Tethys and the Panthalassa; scenario 2 with shallow seaways (shallow ocean) and scenario 3 with closed sea- ways between the Paleo-Tethys and the Panthalassa.

Response of Paleo-Tethys deoxygenation to seaway restriction

Simulation results show that benthic dissolved oxygen concentrations ([O_2]), here calculated as the mean of all benthic grid points, significantly decrease in the Paleo-Tethys with the shallowing or closure of the seaways, dropping from 70 μmol kg^{-1} (scenario 1) to 24 μmol kg^{-1} (scenario 2) and 4 μmol kg^{-1} (scenario 3) (Figs. 3D–F and 4). Regional deoxygenation primarily develops because of the weakening of deep- ocean (> ~1000 m) currents transporting cold and oxygenated waters from the southern Panthalassa to the Paleo-Tethys, as a result of the seaway constriction (Figs. 3A–3C and 5). The resultant decrease in ocean ventilation is evidenced by the development of older benthic water ages in the Paleo-Tethys (Fig. 3G–3I). In addition, seaway restriction pro- motes regional primary productivity in the photic zone (Fig. 3J–3L). This increase of primary productivity arises from the strengthening of equatorial upwelling in the Paleo-Tethys in response to changes in the

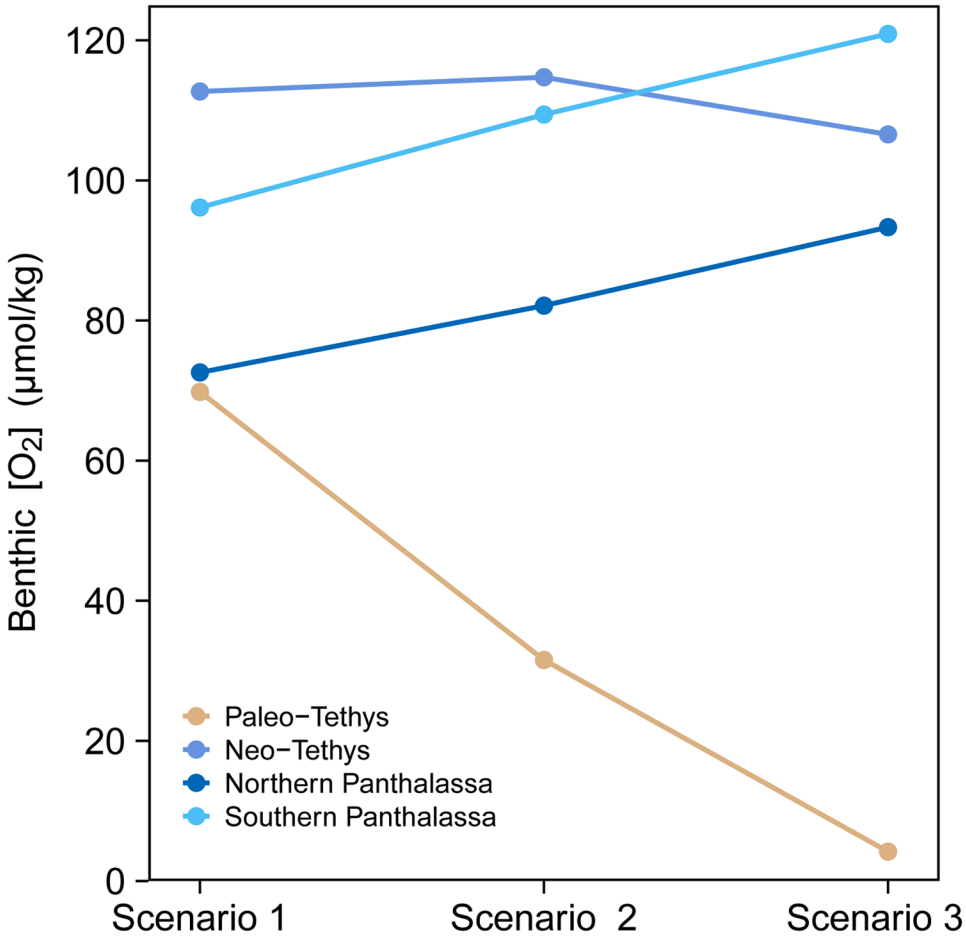

Fig. 4. Comparison of simulated benthic [O_2] in different regions.

regional land-sea distribution, contributing to bringing more nutrients from deeper down to the surface ocean. The increased export production causes a further expansion of anoxic and euxinic conditions in the upper ocean of Paleo-Tethys (Fig. S2). The combined impacts of reduced ocean ventilation and increased primary productivity, in response to seaway restriction, provide an important preconditioning factor to the recur- rence of anoxia in the Paleo-Tethys during the Early to Middle Triassic (Fig. 1), although these seaway restrictions do not explain the precise timing of the frequent anoxic events during the Early-Middle Triassic, as evidenced by multiple shifts of carbon and uranium isotopes and local redox proxies (Fig. 1A). The restricted continental configuration, similar to the modern Black Sea, was also used to explain the development of marine anoxia and black shales during the Devonian-Carboniferous boundary (Hedhli et al., 2023).

Our results indicate a sensitivity to the depth of the seaways between the Paleo-Tethys and the Panthalassa oceans. Sensitivity simulations conducted on scenario 2 demonstrate that, for seaway bathymetries as deep as 1000 m, seafloor [O_2] values in the Paleo-Tethys fall to 20–30 μmol kg^{-1} or less (Fig. 6). This bathymetric threshold corresponds to the minimum depth required for water transport from the Panthalassa to the Paleo-Tethys (Figs. 3A and 5), and its disruption significantly reduces the ventilation in the Paleo-Tethys. Our findings suggest that regional deoxygenation in the Paleo-Tethys is evident in all scenarios, including scenario 1 with very deep seaways (Fig. 3D).

Ocean oxygenation also depends on the global climatic state and oceanic nutrient inventory. Sensitivity analyses demonstrate that our results are robust under variations in temperature and [PO_4] (Fig. 7). This suggests that our modeling mechanism is applicable not only during the earliest Triassic under extremely warm conditions, but could also account for the development of regional marine anoxia in South China during the Early-Middle Triassic transition (e.g., Tian et al. 2014), against a background of cooling climate characterized by a temperature drop of >6 °C (Fig. 1), while most regions lacked marine anoxia records at that time (Fig. 1B).

Notably, these simulations overlook diachronous collisions between blocks and primarily rely on evidence from eastern Paleo-Tethys. Moreover, these methods oversimplify the actual positions and num- ber of blocks around the Paleo-Tethys due to low spatial resolution of the model. Despite its low resolution, cGENIE has been shown to reasonably capture the response of ocean ventilation and oxygenation to seaway bathymetry during the Late Cretaceous oceanic anoxic event 2 (Monteiro et al., 2012), in line with simulations using a higher-resolution model (Laugié et al., 2021). Other factors not accounted for in our modeling, such as different sedimentary facies, local redox conditions or spatial variations in regional nutrient inputs, can also cause variations in ocean redox conditions. However, they do not explain the spatial patterns in marine anoxia documented by redox proxy data. While various anoxic conditions in proximal and distal sedimentary settings are observed during the PTME (Schobben et al., 2020), our seven selected sections all represent distal settings (slope, basin and pelagic domain). For example, sedimentary facies of two sections in Nanpanjiang and Arabian Margin are identified as slope settings, but vary largely in duration and intensity of anoxic conditions (Fig. 1). Additionally, the local redox histories in most regions are reconstructed based on multiple proxies, which overcomes the uncer- tainty that may arise from the use of a single proxy (Fig. 1S).

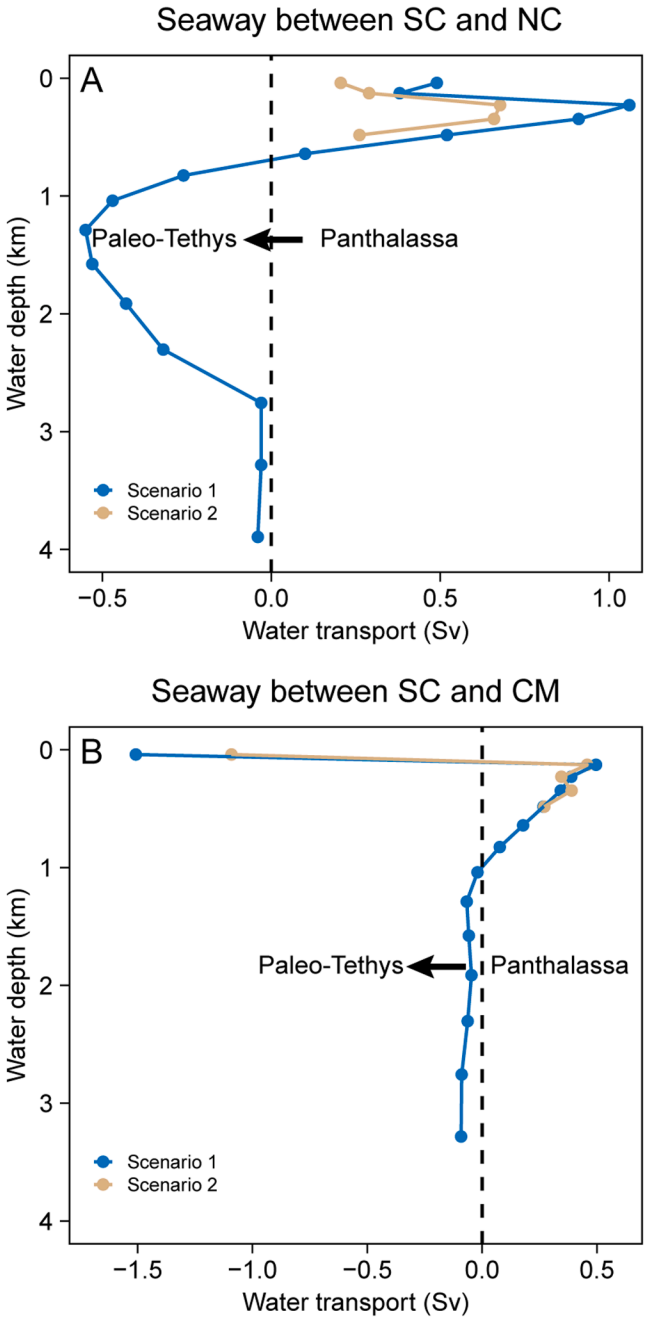

Fig. 5. Water transports across transects of seaways in the eastern Paleo- Tethys. Zonal water transports are computed as in Donnadieu et al. (2016) for: (A) the seaway between South China and North China (see Fig. 3), and (B) the seaway between South China and Cimmerian blocks. Positive values indi- cate eastward transport from the Paleo-Tethys to the Panthalassa. Negative values indicate westward transport from the Panthalassa to the Paleo-Tethys. Westward deep-ocean currents indicated by arrows are developed in the scenario 1, 1 Sv = 10^6 m^3 s^{-1}.

Contrasting response of other regions

The gradual restriction of the seaways also helps explain spatial patterns in ocean redox observed outside the Paleo-Tethys. The seafloor [O_2] of the southern Panthalassa (from 96 to 120 μmol kg^{-1}) and northern Panthalassa (from 73 to 93 μmol kg^{-1}) slightly increase, in response to the weakening or interruption of the transfer of high-[O_2] waters into the Paleo-Tethys (Fig. 4). This global ocean oxygenation offers an explanation for the disappearance of anoxic conditions in most

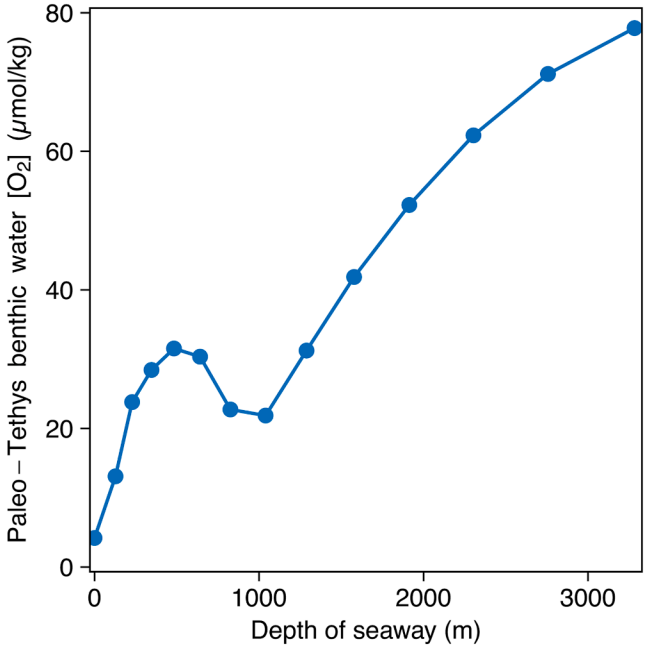

Fig. 6. Sensitivity simulations to seaway depth. Benthic $[O_2]$ in the Paleo- Tethys simulated as a function of the depth of the seaways (the same depth is used for both seaways between SC and NC, SC and CM).

of the Panthalassa after the Early Triassic. In addition, the formation of deep waters in the Panthalassa predominantly occurs at the southern high latitudes (Fig. 3), leading to regional ventilation and oxygenation of the seafloor, while the northern middle-high latitudes remain comparatively less oxygenated (Fig. 3). This likely explains the longer duration of marine anoxia recorded in the Canada Sverdrup basin at the middle latitude of northern Panthalassa compared to New Zealand at the middle latitude of southern Panthalassa (Grasby et al., 2013, 2021) (Fig. 1).

In the Neo-Tethys, simulated $[O_2]$ exhibits minimal sensitivity to the seaway configuration, ranging from 107 to 113 μmol kg^{-1} across our three scenarios (Fig. 4). The muted response is primarily due to the shallower bathymetry in this region (see inset in Fig. 1), rendering the regional $[O_2]$ poorly sensitive to ventilation changes, and the relatively consistent export production (Fig. 3). The high simulated benthic $[O_2]$ in the Neo-Tethys is consistent with redox proxy records indicating that Neo-Tethys became oxic earlier before the Spathian (Fig. 1).

Our simulations fail to capture the recurrent anoxic conditions in central Panthalassa (Japan; Figs. 1 and 3D–F) (Isozaki, 1997; Wignall et al., 2010). This discrepancy between model and data may result from the flat-bottomed ocean used in the simulations, in the absence of geological constraints for the location and geometry of mid-ocean ridges so far back in geological times, since most of the Triassic seafloor has been destroyed in subduction zones. Previous work has demonstrated the significant impact of mid-ocean ridges on regional benthic $[O_2]$ spatial patterns in cGENIE (Pohl et al., 2022). A more complex ba- thymetry in the Panthalassa, including the presence of mid-ocean ridges, might have deflected deep-water currents and thus reduced the venti- lation and oxygenation of seafloor in the central Panthalassa.

Implication for post-crisis recovery

Following the PTME, global marine taxonomic diversity did not rebound to pre-extinction levels until the Middle Triassic (Chen et al., 2012; Song et al., 2020). This protracted recovery is often attributed to recurrent environmental stresses such as anoxic conditions (Song et al., 2012; Grasby et al., 2013; Lau et al., 2016; Zhang et al., 2018a). How- ever, several lines of evidence suggest that the recovery was

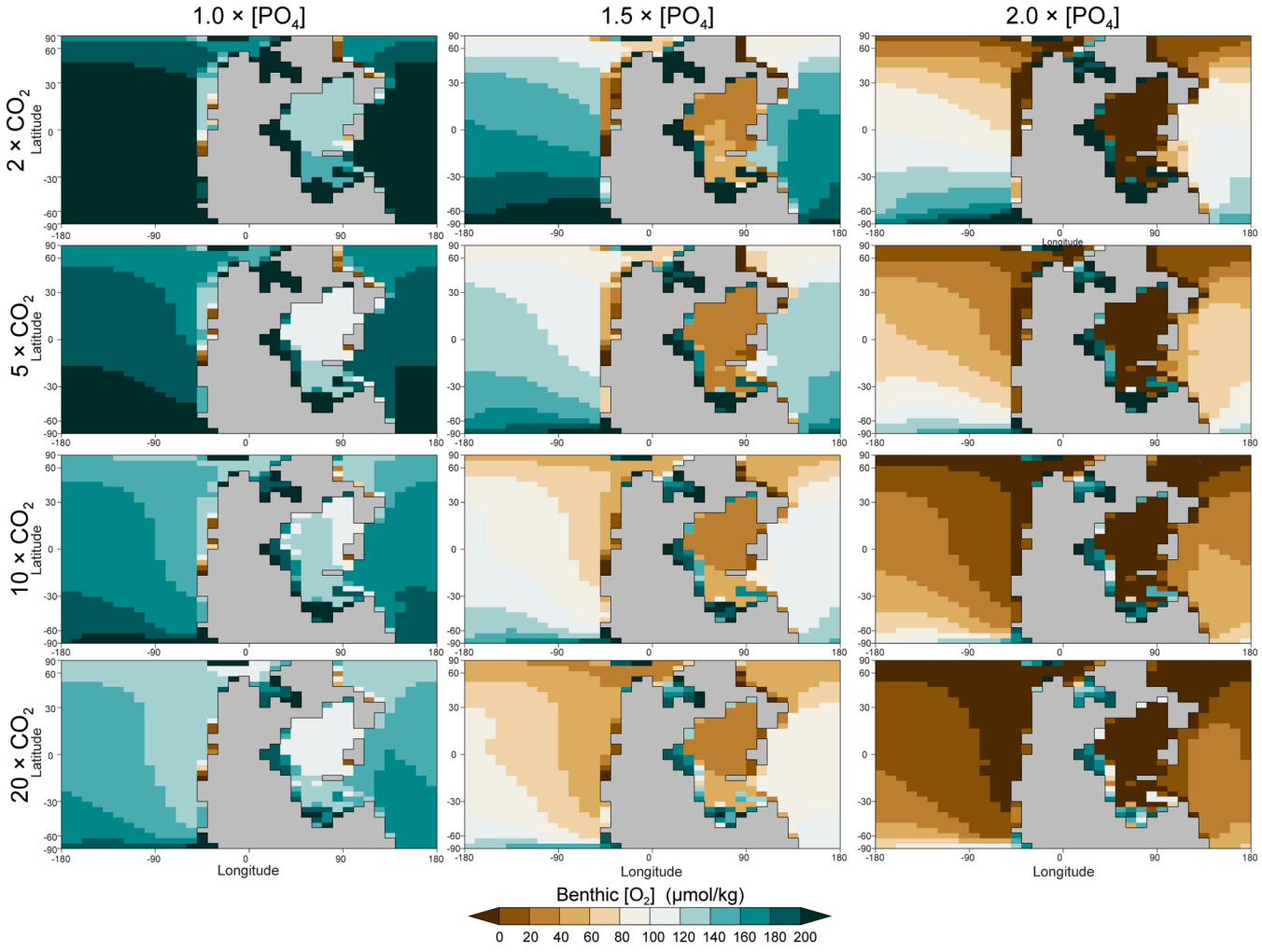

Fig. 7. Sensitivity of benthic [O_2] to atmospheric CO_2 levels and oceanic [PO_4].

asynchronous, with biodiversity increasing more slowly and later in the Paleo-Tethys compared to the Neo-Tethys and the Panthalassa. This pattern is characteristic of the recovery of ammonoids (Brayard et al., 2006, 2009), and radiolarian populations in the southern and northern Panthalassa returned several million years before they did in other re- gions (Grasby et al., 2021; Foster et al., 2023). It is also suggested by flattened latitudinal diversity gradient during the Early Triassic (Song et al., 2020). Specifically, global biodiversity peaks between 30 °N and 15 °S (mostly from Paleo-Tethys) were prominent in the late Permian and Middle Triassic but absent during the Early Triassic, which might be attributed to selective extinction at low latitudes and poleward migra- tion induced by warming (Song et al., 2020). The diachronous spatial recovery cannot be simply attributed to the global environmental stresses (e.g., global warming, marine anoxia) but requires an under- standing of spatial variations in the environmental stresses. Here, we suggest that the spatial variances in the durations and intensities of anoxic conditions, as supported by local redox proxies and our Earth system model simulations, offer one potential explanation for the dia- chronous recovery of marine taxonomic diversity during the Early to Middle Triassic. The recurrent anoxic conditions in the low-latitude Paleo-Tethys, compared to other oceanic regions would have directly impacted marine organisms inhabiting the continental shelves at that time, through the expansion of euxinic waters. Thus, marine taxonomic diversity in the Paleo-Tethys did not rebound to pre-extinction levels until the Middle Triassic, whereas marine taxonomic diversity in some regions recovered more quickly, because lots of regions outside the

Paleo-Tethys returned to healthy oxic systems earlier before the late Early Triassic.

Conclusions

Earth system modeling reveal that shallowing the depth of the sea- ways connecting the Paleo-Tethys and Panthalassa oceans leads to an oxygenation of the seafloor globally, except in the restricted Paleo- Tethys where ocean deoxygenation develops. This modeling spatial pattern of the redox landscape agrees with redox proxy data that show recurrent marine anoxia in the eastern Paleo-Tethys into the Middle Triassic, in contrast to the earlier reoxygenation of other basins (e.g. Neo-Tethys, southern Panthalassa) before the late Early Triassic. Ocean deoxygenation in the Paleo-Tethys mainly arises from the weakening of regional ocean ventilation due to the disruption of deep-water flow across the seaways, in response to seaway restriction. The increased export production resulting from a local increase in equatorial upwelling causes a further expansion of anoxic and euxinic conditions in the upper ocean of Paleo-Tethys. The restricted continental configuration provides an important preconditioning factor to the recurrence of anoxia in the Paleo-Tethys during the Early to Middle Triassic, which could explain the delayed recovery of marine taxonomic diversity in the Paleo-Tethys into the Middle Triassic.

CRediT authorship contribution statement

Yuyang Wu: Writing – original draft, Visualization, Methodology, Investigation, Conceptualization. **Alexandre Pohl:** Writing – review & editing, Visualization, Methodology, Funding acquisition. **Li Tian:** Writing – review & editing, Investigation, Funding acquisition. **Jacopo Dal Corso:** Writing – review & editing, Investigation. **Ying Cui:** Writing

– review & editing, Investigation. **Daoliang Chu:** Writing – review & editing, Investigation. **Jinnan Tong:** Writing – review & editing, Funding acquisition. **Huyue Song:** Writing – review & editing, Investi- gation. **Hanchen Song:** Writing – review & editing, Methodology. **Haijun Song:** Writing – review & editing, Supervision, Investigation, Funding acquisition, Conceptualization.

Declaration of competing interest

The authors declare that they have no known competing financial interests or personal relationships that could have appeared to influence the work reported in this paper.

Data availability

All data used in this study are available in Supplementary material.

Acknowledgements

We thank two anonymous reviewers for their constructive sugges- tions. This study was supported by the National Natural Science Foun- dation of China (92155201, 42030513, 42202002, 42272361,
92255303, 42325202), the State Key R&D Project of China (2023YFF0804000), the Natural Science Foundation of Hubei (2023AFA006), the Fundamental Research Funds for the Central Uni- versities, China University of Geosciences (Wuhan), China Postdoctoral Science Foundation (2021M702997) and State Key Laboratory of Palaeobiology and Stratigraphy (Nanjing Institute of Geology and Palaeontology, CAS) (No. 223132). A.P. acknowledges the support of the French *Agence Nationale de la Recherche* (ANR) under references ANR-22-CE01-0003 (project ECO-BOOST) and of the programme TelluS of the *Institut National des Sciences de l'Univers*, CNRS (project ROSETTA).

Supplementary materials

Supplementary material associated with this article can be found, in the online version, at doi:10.1016/j.epsl.2024.118882.

References

Brayard, A., Bucher, H., Escarguel, G., Fluteau, F., Bourquin, S., Galfetti, T., 2006. The Early Triassic ammonoid recovery: paleoclimatic significance of diversity gradients. Paleogeogr. Paleoclimatol. Paleoecol. 239, 374–395. https://doi.org/10.1016/j. palaeo.2006.02.003.

Brayard, A., Escarguel, G., Bucher, H., Brühwiler, T., 2009. Smithian and Spathian (Early Triassic) ammonoid assemblages from terranes: paleoceanographic and paleogeographic implications. J. Asian Earth Sci. 36, 420–433. https://doi.org/ 10.1016/j.jseaes.2008.05.004.

Brennecka, G.A., Herrmann, A.D., Algeo, T.J., Anbar, A.D., 2011. Rapid expansion of oceanic anoxia immediately before the end-Permian mass extinction. Proc. Natl. Acad. Sci. USA 108, 17631–17634. https://doi.org/10.1073/pnas.1106039108.

Burgess, S.D., Muirhead, J.D., Bowring, S.A., 2017. Initial pulse of Siberian Traps sills as the trigger of the end-Permian mass extinction. Nat. Commun. 8, 164. https://doi. org/10.1038/s41467-017-00083-9.

Chen, Z.Q., Benton, M.J., 2012. The timing and pattern of biotic recovery following the end-Permian mass extinction. Nat. Geosci. 5, 375–383. https://doi.org/10.1038/ ngeo1475.

Clarkson, M.O., Wood, R.A., Poulton, S.W., Richoz, S., Newton, R.J., Kasemann, S.A., Bowyer, F., Krystyn, L., 2016. Dynamic anoxic ferruginous conditions during the end-Permian mass extinction and recovery. Nat. Commun. 7, 12236. https://doi. org/10.1038/ncomms12236.

Crichton, K.A., Wilson, J.D., Ridgwell, A., Pearson, P.N., 2021. Calibration of temperature-dependent ocean microbial processes in the cGENIE.muffin (v0.9.13) Earth system model. Geosci. Model Dev. 14, 125–149. https://doi.org/10.5194/ gmd-14-125-2021.

Donnadieu, Y., Pucéat, E., Moiroud, M., Guillocheau, F., Deconinck, J.F., 2016. A better-
ventilated ocean triggered by Late Cretaceous changes in continental configuration. Nat. Commun. 7, 10316. https://doi.org/10.1038/ncomms10316.

Duan, L., Meng, Q.R., Wu, G.L., Yang, Z., Wang, J., Zhan, R., 2020. Nanpanjiang basin: a window on the tectonic development of south China during Triassic assembly of the southeastern and eastern Asia. Gondwana Res. 78, 189–209. https://doi.org/ 10.1016/j.gr.2019.08.009.

Edwards, N., Marsh, R., 2005. Uncertainties due to transport-parameter sensitivity in an efficient 3-D ocean-climate model. Clim. Dyn. 24, 415–433. https://doi.org/ 10.1007/s00382-004-0508-8.

Elrick, M., Polyak, V., Algeo, T.J., Romaniello, S., Asmerom, Y., Herrmann, A.D., Anbar, A.D., Zhao, L., Chen, Z.Q., 2017. Global-ocean redox variation during the middle-late Permian through Early Triassic based on uranium isotope and Th/U trends of marine carbonates. Geology 45, 163–166. https://doi.org/10.1130/ G38585.1.

Feng, Z.Z., Bao, Z.D., Li, S.W., 1997. Lithofacies Paleogeography of Middle and Lower Triassic of South China. Petroleum Industry Press, Beijing. Chinese with English abstract.

Foster, W.J., Asatryan, G., Rauzi, S., Botting, J.P., Buchwald, S.Z., Lazarus, D.B., Isson, T., Renaudie, J., Kiessling, W., 2023. Response of siliceous marine organisms to the Permian-Triassic climate crisis based on new findings From central Spitsbergen, Svalbard. Paleoceanogr. Paleoclimatol. 38 https://doi.org/10.1029/2023PA004766 e2023PA004766.

Grasby, S.E., Beauchamp, B., Embry, A., Sanei, H., 2013. Recurrent Early Triassic ocean anoxia. Geology 41, 175–178. https://doi.org/10.1130/G33599.1.

Grasby, S.E., Bond, D.P.G., Wignall, P.B., Yin, R., Strachan, L.J., Takahashi, S., 2021. Transient Permian-Triassic euxinia in the southern Panthalassa deep ocean. Geology 49, 889–893. https://doi.org/10.1130/G48928.1.

Hedhli, M., Grasby, S.E., Henderson, C.M., Davis, B.J., 2023. Multiple diachronous "Black Seas" mimic global ocean anoxia during the latest Devonian. Geology 51, 973–977. https://doi.org/10.1130/G51394.1.

Hu, F., Liu, S., Ducea, M.N., Chapman, J.B., Wu, F., Kusky, T., 2020. Early Mesozoic magmatism and tectonic evolution of the Qinling Orogen: implications for oblique continental collision. Gondwana Res. 88, 296–332. https://doi.org/10.1016/j. gr.2020.07.006.

Hu, Z., Li, W., Zhang, H., Krainer, K., Zheng, Q.F., Xia, Z., Hu, W., Shen, S.Z., 2021. Mg isotope evidence for restriction events within the Paleotethys ocean around the Permian-Triassic transition. Earth Planet. Sci. Lett. 556, 116704 https://doi.org/ 10.1016/j.epsl.2020.116704.

Huang, B., Yan, Y., Piper, J.D.A., Zhang, D., Yi, Z., Yu, S., Zhou, T., 2018. Paleomagnetic constraints on the paleogeography of the East Asian blocks during Late Paleozoic and Early Mesozoic times. Earth Sci. Rev. 186, 8–36. https://doi.org/10.1016/j. earscirev.2018.02.004.

Huang, Y., Chen, Z.Q., Wignall, P.B., Zhao, L., 2017. Latest Permian to Middle Triassic redox condition variations in ramp settings, South China: pyrite framboid evidence. Geol. Soc. Am. Bull. 129, 229–243. https://doi.org/10.1130/B31458.1.

Hülse, D., Lau, K.V., van de Velde, S.J., Arndt, S., Meyer, K.M., Ridgwell, A., 2021. End- Permian marine extinction due to temperature-driven nutrient recycling and euxinia. Nat. Geosci. 14, 862–867. https://doi.org/10.1038/s41561-021-00829-7.

Isozaki, Y., 1997. Permo-Triassic boundary superanoxia and stratified superocean: records from lost deep sea. Science 276, 235–238. https://doi.org/10.1126/ science.276.5310.235.

Joachimski, M.M., Müller, J., Gallagher, T.M., Mathes, G., Chu, D.L., Mouraviev, F., Silantiev, V., Sun, Y.D., Tong, J.N., 2022. Five million years of high atmospheric CO_2 in the aftermath of the Permian-Triassic mass extinction. Geology 50, 650–654. https://doi.org/10.1130/G49714.1.

Kiehl, J.T., Shields, C.A., 2005. Climate simulation of the latest Permian: implications for mass extinction. Geology 33, 757. https://doi.org/10.1130/G21654.1.

Lau, K.V., Maher, K., Altiner, D., Kelley, B.M., Kump, L.R., Lehrmann, D.J., Silva- Tamayo, J.C., Weaver, K.L., Yu, M., Payne, J.L., 2016. Marine anoxia and delayed Earth system recovery after the end-Permian extinction. Proc. Natl. Acad. Sci. USA 113, 2360–2365. https://doi.org/10.1073/pnas.1515080113.

Laugié, M., Donnadieu, Y., Ladant, J.B., Bopp, L., Ethé, C., Raisson, F., 2021. Exploring the impact of cenomanian paleogeography and marine gateways on oceanic oxygen. Paleoceanogr. Paleoclimatol. 36 https://doi.org/10.1029/2020PA004202 e2020PA004202.

Li, H., Wignall, P.B., Jiang, H., Zhang, M., Wu, X., Lai, X., 2023. A review of carbon isotope excursions, redox changes and marine red beds of the Early Triassic with insights from the Qinling Sea, northwest China. Earth Sci. Rev. 247, 104623 https:// doi.org/10.1016/j.earscirev.2023.104623.

Metcalfe, I., 2021. Multiple Tethyan ocean basins and orogenic belts in Asia. Gondwana Res. 100, 87–130. https://doi.org/10.1016/j.gr.2021.01.012.

Meyer, K.M., Kump, L.R., Ridgwell, A., 2008. Biogeochemical controls on photic-zone euxinia during the end-Permian mass extinction. Geology 36, 747–750. https://doi. org/10.1130/G24618A.1.

Meyer, K.M., Ridgwell, A., Payne, J.L., 2016. The influence of the biological pump on ocean chemistry: implications for long-term trends in marine redox chemistry, the global carbon cycle, and marine animal ecosystems. Geobiology 14, 207–219. https://doi.org/10.1111/gbi.12176.

Monteiro, F.M., Pancost, R.D., Ridgwell, A., Donnadieu, Y., 2012. Nutrients as the dominant control on the spread of anoxia and euxinia across the Cenomanian-
Turonian oceanic anoxic event (OAE2): model-data comparison. Paleoceanography 27, PA4209. https://doi.org/10.1029/2012PA002351.

Payne, J.L., Lehrmann, D.J., Wei, J., Orchard, M.J., Schrag, D.P., Knoll, A.H., 2004. Large perturbations of the carbon cycle during recovery from the end-Permian extinction. Science 305, 506–509. https://doi.org/10.1126/science.1097023.

Penn, J.L., Deutsch, C., Payne, J.L., Sperling, E.A., 2018. Temperature-dependent hypoxia explains biogeography and severity of end-Permian marine mass extinction. Science 362, eaat1327. https://doi.org/10.1126/science.aat1327.

Pohl, A., Ridgwell, A., Stockey, R.G., Thomazo, C., Keane, A., Vennin, E., Scotese, C.R., 2022. Continental configuration controls ocean oxygenation during the Phanerozoic. Nature 608, 523–527. https://doi.org/10.1038/s41586-022-05018-z.

Ridgwell, A., Hargreaves, J.C., Edwards, N.R., Annan, J.D., Lenton, T.M., Marsh, R., Yool, A., Watson, A., 2007. Marine geochemical data assimilation in an efficient Earth System Model of global biogeochemical cycling. Biogeosciences 4, 87–104. https://doi.org/10.5194/bg-4-87-2007.

Saito, R., Oba, M., Kaiho, K., Schaeffer, P., Adam, P., Takahashi, S., Watanabe Nara, F., Chen, Z.Q., Tong, J., Tsuchiya, N., 2014. Extreme euxinia just prior to the Middle Triassic biotic recovery from the latest Permian mass extinction. Org. Geochem. 73, 113–122. https://doi.org/10.1016/j.orggeochem.2014.05.007.

Schobben, M., Foster, W.J., Sleveland, A.R.N., Zuchuat, V., Svensen, H.H., Planke, S., Bond, D.P.G., Marcelis, F., Newton, R.J., Wignall, P.B., Poulton, S.W., 2020. A nutrient control on marine anoxia during the end-Permian mass extinction. Nat. Geosci. 13, 640–646. https://doi.org/10.1038/s41561-020-0622-1.

Scotese, C.R., 2021. An atlas of Phanerozoic paleogeographic maps: the seas come in and the seas go out. Annu. Rev. Earth Planet. Sci. 49, 679–728. https://doi.org/10.1146/ annurev-earth-081320-064052.

Şengör, A.M.C., Atayman, S., 2009. The Permian extinction and the Tethys: an exercise in global geology. Geol. Soc. Am. Spec. Pap. 448, 57. https://doi.org/10.1130/ 2009.2448.

Song, H.J., Huang, S., Jia, E.H., Dai, X., Wignall, P.B., Dunhill, A.M., 2020. Flat latitudinal diversity gradient caused by the Permian–Triassic mass extinction. Proc. Natl. Acad. Sci. USA 117, 17578. https://doi.org/10.1073/pnas.1918953117.

Song, H.J., Wignall, P.B., Tong, J., Bond, D.P.G., Song, H.Y., Lai, X., Zhang, K., Wang, H., Chen, Y., 2012. Geochemical evidence from bio-apatite for multiple oceanic anoxic events during Permian–Triassic transition and the link with end-Permian extinction and recovery. Earth Planet. Sci. Lett. 353-354, 12–21. https://doi.org/10.1016/j. epsl.2012.07.005.

Song, H.Y., Tong, J.N., Algeo, T.J., Horacek, M., Qiu, H., Song, H.J., Tian, L., Chen, Z.Q., 2013. Large vertical $\delta^{13}C$ DIC gradients in Early Triassic seas of the South China craton: implications for oceanographic changes related to Siberian Traps volcanism. Glob. Planet. Chang. 105, 7–20. https://doi.org/10.1016/j.gloplacha.2012.10.023.

Sun, Y.D., Joachimski, M.M., Wignall, P.B., Yan, C.B., Chen, Y.L., Jiang, H.S., Wang, L.N., Lai, X.L., 2012. Lethally hot temperatures during the Early Triassic greenhouse. Science 338, 366–370. https://doi.org/10.1126/science.1224126.

Sun, Y.D., Richoz, S., Krystyn, L., Grasby, S.E., Chen, Y.L., Banerjee, D., Joachimski, M. M., 2021. Integrated bio-chemostratigraphy of lower and middle triassic marine successions at spiti in the Indian Himalaya: implications for the Early Triassic nutrient crisis. Glob. Planet. Chang. 196, 103363 https://doi.org/10.1016/j. gloplacha.2020.103363.

Takahashi, S., Oba, M., Kaiho, K., Yamakita, S., Sakata, S., 2009. Panthalassic oceanic anoxia at the end of the Early Triassic: a cause of delay in the recovery of life after the end-Permian mass extinction. Paleogeogr. Paleoclimatol. Paleoecol. 274, 185–195. https://doi.org/10.1016/j.palaeo.2009.01.010.

Takahashi, S., Yamasaki, S., Ogawa, K., Kaiho, K., Tsuchiya, N., 2015. Redox conditions in the end-Early Triassic Panthalassa. Paleogeogr. Paleoclimatol. Paleoecol. 432, 15–28. https://doi.org/10.1016/j.palaeo.2015.04.018.

Tian, L., Tong, J., Algeo, T.J., Song, H., Song, H., Chu, D., Shi, L., Bottjer, D.J., 2014. Reconstruction of Early Triassic ocean redox conditions based on framboidal pyrite from the Nanpanjiang Basin, South China. Paleogeogr. Paleoclimatol. Paleoecol. 412, 68–79. https://doi.org/10.1016/j.palaeo.2014.07.018.

Tong, J., Chu, D., Liang, L., Shu, W., Song, H., Song, T., Song, H., Wu, Y.Y., 2019. Triassic integrative stratigraphy and timescale of China. Sci. China Earth Sci. 62, 189–222. https://doi.org/10.1007/s11430-018-9278-0.

Tong, J.N., Chu, D.L., Miao, X., Shu, W., Guo, W., Wu, Y., Su, Y., Wu, K., Ji, K.X., Yu, Y. Y., 2021. Lithostratigraphic subdivision and correlation of the Triassic in China. J. Stratigr. 45, 340–363. https://doi.org/10.19839/j.cnki.dcxzz.2021.0028 in Chinese with English abstract.

Trotter, J.A., Williams, I.S., Nicora, A., Mazza, M., Rigo, M., 2015. Long-term cycles of Triassic climate change: a new $\delta^{18}O$ record from conodont apatite. Earth Planet. Sci. Lett. 415, 165–174. https://doi.org/10.1016/j.epsl.2015.01.038.

Wang, Y., Qian, X., Cawood, P.A., Liu, H., Feng, Q., Zhao, G., Zhang, Y., He, H., Zhang, P., 2018. Closure of the East Paleotethyan Ocean and amalgamation of the Eastern Cimmerian and Southeast Asia continental fragments. Earth Sci. Rev. 186, 195–230. https://doi.org/10.1016/j.earscirev.2017.09.013.

Wignall, P.B., Bond, D.P.G., Kuwahara, K., Kakuwa, Y., Newton, R.J., Poulton, S.W., 2010. An 80 million year oceanic redox history from Permian to Jurassic pelagic sediments of the Mino-Tamba terrane, SW Japan, and the origin of four mass extinctions. Glob. Planet. Chang. 71, 109–123. https://doi.org/10.1016/j. gloplacha.2010.01.022.

Winguth, C., Winguth, A.M.E., 2012. Simulating Permian–Triassic oceanic anoxia distribution: implications for species extinction and recovery. Geology 40, 127–130. https://doi.org/10.1130/G32453.1.

Wu, Y.Y., Cui, Y., Chu, D.L., Song, H.J., Tong, J.N., Dal Corso, J., Ridgwell, A., 2023. Volcanic CO_2 degassing postdates thermogenic carbon emission during the end- Permian mass extinction. Sci. Adv. 9, eabq4082. https://doi.org/10.1126/sciadv. abq4082.

Zhang, F., Algeo, T.J., Cui, Y., Shen, J., Song, H., Sano, H., Rowe, H.D., Anbar, A.D., 2019. Global-ocean redox variations across the Smithian-Spathian boundary linked to concurrent climatic and biotic changes. Earth-Sci. Rev. 195, 147–168. https://doi. org/10.1016/j.earscirev.2018.10.012.

Zhang, F., Algeo, T.J., Romaniello, S.J., Cui, Y., Zhao, L., Chen, Z.Q., Anbar, A.D., 2018b. Congruent Permian-Triassic $\delta^{238}U$ records at Panthalassic and Tethyan sites: confirmation of global-oceanic anoxia and validation of the U-isotope paleoredox proxy. Geology 46, 327. https://doi.org/10.1130/G39695.1.

Zhang, F., Shen, S.Z., Cui, Y., Lenton, T.M., Dahl, T.W., Zhang, H., Zheng, Q.F., Wang, W., Krainer, K., Anbar, A.D., 2020. Two distinct episodes of marine anoxia during the Permian-Triassic crisis evidenced by uranium isotopes in marine dolostones. Geochim. Cosmochim. Acta 287, 165–179. https://doi.org/10.1016/j. gca.2020.01.032.

Zhang, F., Romaniello, S.J., Algeo, T.J., Lau, K.V., Clapham, M.E., Richoz, S., Herrmann, A.D., Smith, H., Horacek, M., Anbar, A.D., 2018a. Multiple episodes of extensive marine anoxia linked to global warming and continental weathering following the latest Permian mass extinction. Sci. Adv. 4, e1602921 https://doi.org/ 10.1126/sciadv.1602921.

Zhao, H., Algeo, T.J., Liu, Y., Chen, Z.Q., Zhang, L., Hu, Z., Li, Z., 2020. Lower Triassic carbonate $\delta^{238}U$ record demonstrates expanded oceanic anoxia during Smithian Thermal Maximum and improved ventilation during Smithian-Spathian boundary cooling event. Paleogeogr. Paleoclimatol. Paleoecol. 539, 109393 https://doi.org/ 10.1016/j.palaeo.2019.109393.

Zhu, R., Zhao, P., Zhao, L., 2022. Tectonic evolution and geodynamics of the Neo-Tethys Ocean. Sci. China-Earth Sci. 65, 1–24. https://doi.org/10.1007/s11430-021-9845-7.